Fluid Dynamics & Materials Processing

Tech Science Press

DOI: 10.32604/fdmp.2022.021793

ARTICLE

Hydrodynamic Pattern Investigation of Ethanol Droplet Train Impingement on Heated Aluminum Surface

Baris Burak Kanbur, Sheng Quan Heng and Fei Duan*

School of Mechanical and Aerospace Engineering, Nanyang Technological University, 639798, Singapore

*Corresponding Author: Fei Duan. Email: feiduan@ntu.edu.sg

Received: 04 February 2022 Accepted: 25 February 2022

ABSTRACT

Steady-state hydrodynamic patterns of ethanol droplet train impingement on the heated aluminum surface is investigated in the surface temperature range of 80°C–260°C using two different Weber numbers (We) of 618 and 792. Instead of a vertical train impingement, the droplet train is sent to the aluminum surface with an incline of 63 degrees. Changes in the spreading length are observed at different surface temperatures for two different We values, which are obtained by using two different pinholes with 100 and 150 μm diameters. The greatest spreading length is seen at the lowest surface temperature (80°C) and it continuously decreases until the surface temperature of 200°C. Above 200°C, the spreading length remains stable which is most probably because of the Leidenfrost effect. The spreading lengths of the experiments with 100 μm are 46.4% smaller than the experiments with 150 μm. Also, splashing angles are observed for both We values. The ranges of splashing angle observations are 140°C–200°C and 170°C–185°C for We values of 792 and 618, respectively.

KEYWORDS

Hydrodynamic patterns; boiling; droplet spreading; two phase flow; heat transfer

Nomenclature

d	Droplet diameter in air, mm
D	Droplet nozzle, μm
f	Frequency, kHz
l	Spacing between adjacent droplets, mm
T	Temperature, °C
Re	Reynolds number
w	Surface wall
We	Weber number
ν	Droplet velocity, m/s
μ	Viscosity, Pa·s
ρ	Density, kg/m^3
σ	Surface tension, N/m

1 Introduction

The droplet train impingement technique is an advanced approach of the droplet impingement studies to better analyze the boiling behaviors of the liquid impinged on the substrate [1]. In addition to the single droplet train impingement-related observations like wetting and oscillation, the droplet train impingement can provide an observational environment for investigating the spreading length, splashing angles, splashing directions, and crown formation [2]. Hereby, the train impingement works can better mimic the real and complex boiling phenomena in advanced engineering applications that vary from heating & cooling to additive manufacturing [3,4]. Up to now, various droplet train impingement studies have been applied with low- or high-frequency, low- or high-Weber number, or single or multiple trains [5–9]. Furthermore, our group has been performing droplet train impingement studies on the heated surfaces via DI water or ethanol to better characterize the boiling trends and the Leidenfrost regime [10–13]. However, the number of droplet train impingement studies are still limited compared to the well-established single droplet impingement studies; hence, there are still important research gaps for a better understanding of train impingement behaviors for various surfaces via different liquids. The investigation of inclined droplet train impingement on a target surface is one of the gap areas so that our main contribution is to investigate the impact of an inclined ethanol droplet train impingement on an aluminum surface with two different pinhole diameters; 100 and 150 μm. The ethanol (liquid)-aluminum (substrate) couple is selected because both are widely applied in thermal engineering studies and their combined investigations have been very limited up to now. The incline of the droplet train is adjusted to 63 degrees and the aluminum surface temperature ranges between 80°C–260°C.

2 Experimental Setup

The experimental setup includes an ethanol liquid-filled stainless-steel tank (pressurized via compressed air), a flow meter and a pressure sensor for ethanol flow measurements, a piezoelectric ceramic element and function generator for generating droplets from the ethanol flow, droplet nozzle that includes pinholes at the micrometer scale, high-speed camera for optical imaging, a light source for the effective operation of the high-speed camera, desktop computer for data logging, cylindrical heating cartridge for heating power to the insulated copper that heats the substrate temperature, and aluminum substrate. The simplified figure is presented in Fig. 1.

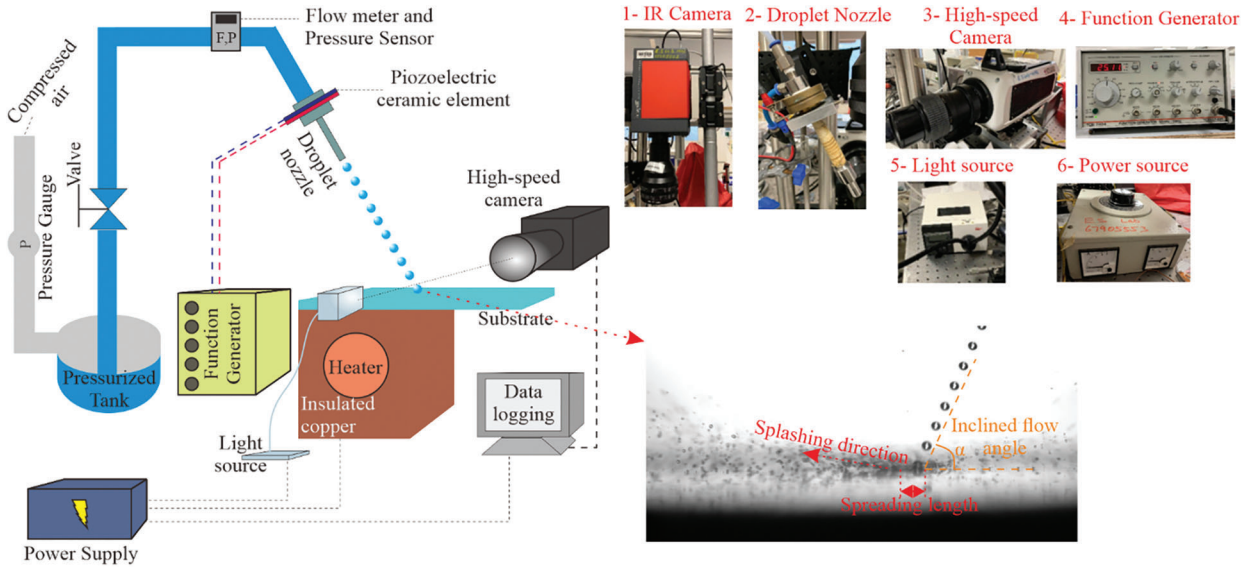

Figure 1: Simplified schematic of the ethanol droplet train impingement system

Ethanol (purity ≥ 99.9%; density = 789 kg/m^3; surface tension = 0.022 N/m; dynamic viscosity = 0.012 Pa·s; and boiling temperature = 78.4°C) was obtained from Sigma-Aldrich. Its temperature is 26°C before impinging on the surface. The droplet generator system (FMP Technology GmbH, Germany) is a component that also includes the piezoelectric ceramic element. The high-speed camera is Phantom V711 model with 1024 × 512 resolution and we collected images with 14000 frames per second and 1 μs exposure time. Also, Canon MP-E 65 lens with 2X magnification was applied in the experiments. The light source model is Leica CLS150 LED. As shown in Fig. 1, the aluminum substrate is not fully placed onto the copper block; instead, partially located. The reason behind this placement is to create small temperature gradients on the aluminum surface because the vast majority of existing droplet train impingement studies have been performed on the target surface with a constant temperature. However, in many real applications, the surface has temperature gradients so that we create a small temperature gradient before impinging the ethanol droplet train onto the surface. On the right side of Fig. 1, an illustrative example of the collected optical image is shown during the experiments. The ethanol flow has an incline of 63 degrees. After the first impingement, the continuous droplet train generates an impact area and crater region. To characterize the drop impact, spreading length is preferred. According to the surface energy levels, which mostly depend on the surface temperature, uniform and continuous splashing can be observed. In the case of splashing observation with a uniform direction, the splashing angle can be measured. The surface temperature measurements were done via thermal imaging and thermocouples (from multiple locations of the substrate); then, the collected temperature values were calibrated. To define the physical properties of the generated droplets, Weber (We) and Reynolds (Re) numbers can be used as shown below:

$$\mathrm{We} = (\rho \cdot \nu^2 \cdot \mathrm{d}) / \sigma \tag{1}$$

$$\mathrm{Re} = (\rho \cdot \nu \cdot \mathrm{d}) / \mu \tag{2}$$

where ρ is the density of the ethanol, ν is the droplet velocity, d is the droplet diameter in the air, σ is the surface tension, and μ is the viscosity. In this study, we prefer defining the generated droplet trains only using We value. The overall characteristics of the generated droplets in two different experiments are shown in Table 1. The reason behind the differences in We values is the pinhole diameter (D_0) value while other parameters are very close to one another. The obtained difference in We values is the desired fact since we would like to see the impact of different We and D_0 values on the boiling performance.

Table 1: Main characteristics of droplet impingement

Droplet parameters	Experiment A	Experiment B
D_0 (μm)	100	150
d (mm)	0.16	0.2
l (mm)	0.41	0.42
f (kHz)	25.0	25.1
We	618	792

3 Results and Discussion

The impact of the droplet train impingement on the target surface can be evaluated with the spreading length, splashing angle, boiling bubbles, and/or crown formation [11,12]. All of these phenomena are related to the thermal balance between the liquid ethanol supply to the surface and the surface energy level. The surface energy level is mostly based on the surface temperature and roughness value; however, if two

different substrates are compared to each other, thermal conductivity should also be considered. In this study, the target surface is the same aluminum plate so that the surface energy level depends on only the surface temperature. When the surface temperature increases, the surface energy level grows up and it provides a higher evaporation rate. A high evaporation rate achieves a smaller droplet impact area that can affect the spreading length and splashing angle. Thus, it is known that lower surface temperature values result in greater spreading length. In Fig. 2, the steady-state hydrodynamic patterns of the inclined ethanol droplet train impingement experiments are shown at the surface temperature values of 80°C and 110°C.

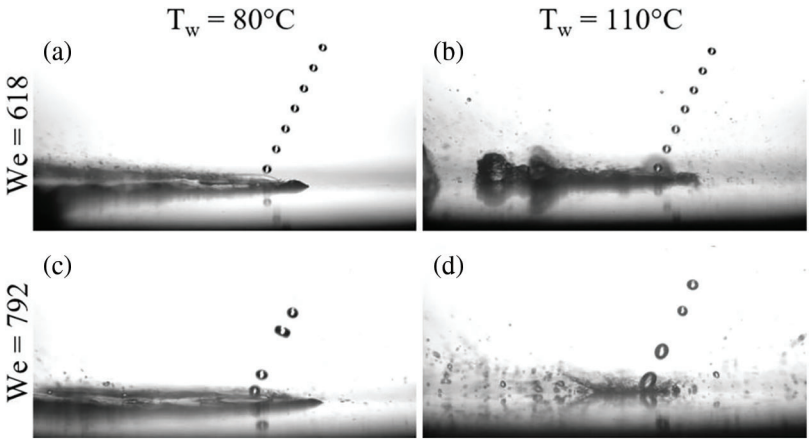

Figure 2: Steady-state hydrodynamic patterns of the inclined ethanol droplet train impingement experiments at the surface temperature values of 80°C and 110°C

Even though the surface temperature values are greater than the boiling point of the ethanol (78.4°C), the surface energy level is not enough for sufficient evaporation at 80°C for both Experiments A and B due to the small temperature difference between the wall temperature and the boiling point. Thus, the ethanol liquid flows on the target surface with a low evaporation rate and a large liquid accumulation is observed. However, the increase of surface temperature to 110°C improves the surface energy level and the evaporation rate increases. Thanks to this increment, Experiment A (We = 618) has some nucleate boiling bubbles near the droplet impact area, which is a sign of nucleate boiling regime as also mentioned in [11,12,14]. For Experiment B (We = 792), the higher ethanol supply (due to D_0 and d in Table 1) results in non-uniform splashed microdroplets, which is a sign of splashing phenomenon [11,12,14]. The splashing phenomenon is an important term of the thermal balance between the liquid supply and the surface energy. Like a higher evaporation rate, the observation of splashing phenomena also means that the surface energy is high enough to break large ethanol droplets into microdroplets (splashed droplets in Fig. 2). Following the droplet hydrodynamic behaviors from 80°C to 110°C, Fig. 3 shows the steady-state hydrodynamic patterns in the surface temperature ranges of 140°C–200°C.

It is seen that the spreading length has a decrement trend from 140°C to 200°C since the increase of surface temperature provides a higher surface energy level that improves the evaporation rate. The increase of surface temperature also makes the splashed droplets more appear for both Experiments A and B. For Experiment A, the splashed droplets are still moving nonuniformly at 140°C; however, it has a uniform direction between 170°C and 185°C. Thus, the uniform splashing direction is marked as the splashing angle and it is seen that the splashing angle increases from 170°C to 185°C. However, the splashing angle decreases between 185°C and 200°C and the angle value is nearly zero at the temperature of 200°C. That is to say, during the real process, the splashing angle first appears between 140°C and 170°C and ends between 185°C and 200°C, but we cannot know the exact surface temperature values for

the start and end since they are not in our observation temperature values. For Experiment B, the splashing angle starts between 110°C and 140°C because we can clearly see a uniform splashing direction at the temperature of 140°C, unlike Experiment A. The splashing angle increases up to 170°C; and stays nearly constant till 185°C. At 200°C, the splashing angle value is lower than the angle at 185°C; thus, we can say that the decrement starts after 185°C. At 215°C, the splashing angle becomes nearly zero. According to [11–14], the observation of splashing angles is a sign of transition regime, and it is expected to see the decrement of splashing angle in the transition regime. Therefore, we can state that Experiment A is exactly in the boiling regime between 80°C and 170°C; then, the sign of transition regime is observed between 170°C and 185°C; and the transition regime is defined between 185°C and 200°C. For Experiment B, the boiling regime is between 80°C and 140°C; the sign of transition is between 140°C and 170°C, and the transition regime is between 185°C and 215°C. The calculated splashing angles can be seen in Fig. 4.

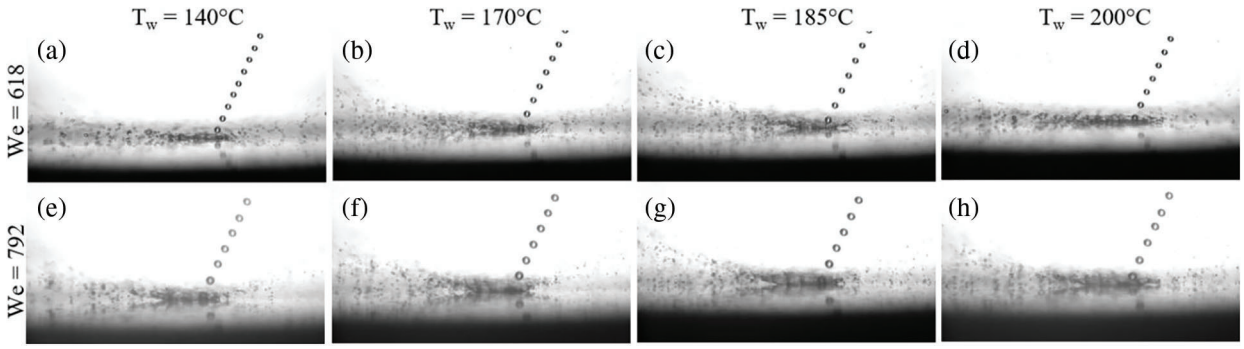

Figure 3: Steady-state hydrodynamic patterns of the inclined ethanol droplet train impingement experiments at the surface temperature values between 140°C and 200°C

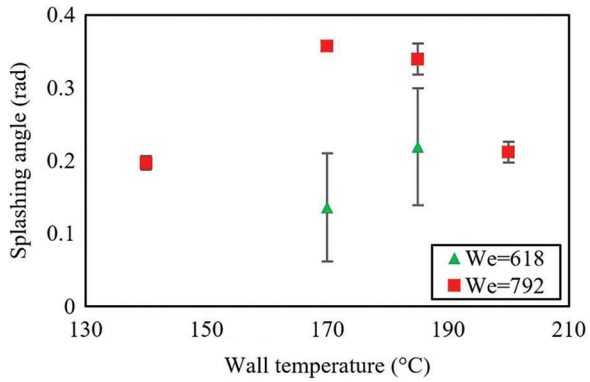

Figure 4: Splashing angles at the surface temperature values between 140°C and 200°C (error bars obtained from two times repeated experiments)

The post-transition regime is defined as the regime that follows the end of the transition regime. The hydrodynamic patterns at the post-transition regime are shown until the surface temperature of 260°C for both Experiments A and B in Fig. 5. In the post-transition regime, spreading lengths are smaller compared to lower surface temperature values since higher surface temperatures provide a higher surface energy level. In Fig. 5, it is seen that both experiments have chaotic micro splashes from the impingement point. Spreading length remains nearly constant and does not decrease, but it is also a fact

that the measured splashing length is around 0.2 and 0.4 mm for Experiments A and B, respectively, which are very close to the droplet in air (d) value in Table 1. Reaching these small values states that the aluminum provides a very high surface energy level, which is also related to its high thermal conductivity, and therefore, the evaporation rate becomes very high to keep the spreading length as small as possible. On the other hand, the observed splashes do not have a continuous and uniform direct like in the splashing angle trends, but the collected images are similar to the observed splashes at high temperatures (above 200°C) in [13,14]. As mentioned in [13,14], the end of the transition regime can be related to the fingering boiling [15], which is a sign of the Leidenfrost point. Therefore, following the observational outcomes of [13–15] and considering the stable spreading lengths and the end of transition regime, we can deduce that both experiments reach the Leidenfrost point above 200°C, but Experiment A reaches earlier (see Fig. 4). This is related to the lower ethanol liquid supply that allows the substrate to make the thermal balance (via surface energy level) at a smaller spreading length with a high evaporation rate.

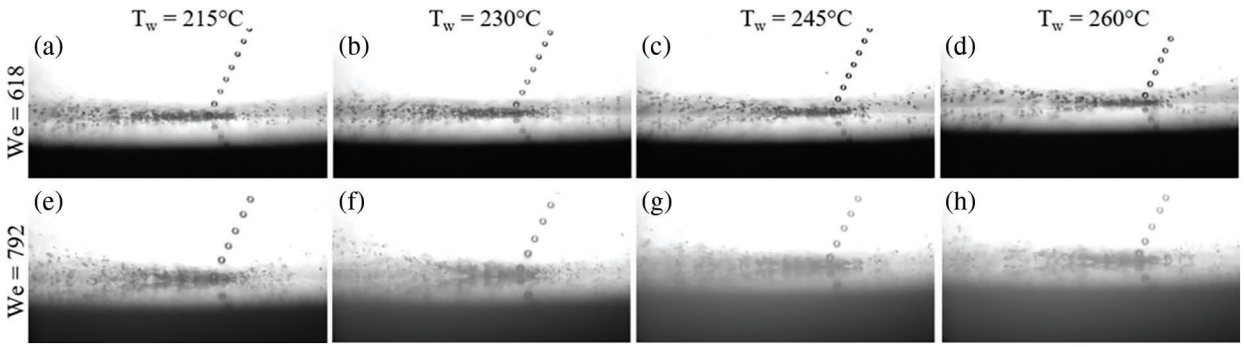

Figure 5: Steady-state hydrodynamic patterns of the inclined ethanol droplet train impingement experiments at the surface temperature values between 215°C and 260°C

After mentioning the steady-state hydrodynamic patterns at various surface temperature values, the decrease trends of spreading lengths are plotted in Fig. 6 for both Experiments A and B. Due to the higher ethanol supply rate and higher droplet in air diameter (d), Experiment B has greater spreading lengths, inherently. In a general comparison, Experiment A has nearly 46.4% smaller spreading lengths than Experiment B. In addition, from 80°C to 260°C, the spreading length decreases by 72.44% and 51.02% in Experiments A and B, respectively. This huge decrement shows the impact of surface temperature.

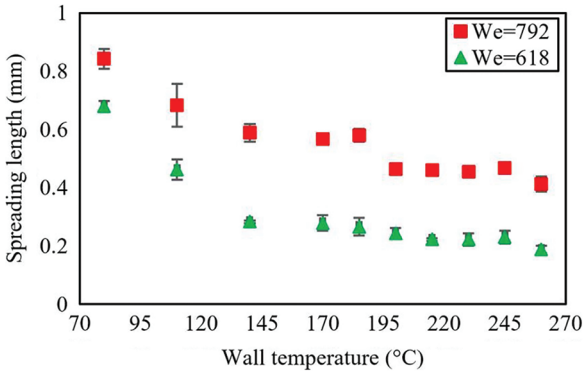

Figure 6: Spreading lengths at the surface temperature values between 215°C and 260°C (error bars obtained from two times repeated experiments)

4 Conclusions

In this study, the optical investigation of the ethanol droplet train impingement on the aluminum surface was done with two different Weber numbers: 618 and 792. The droplet train had an incline of 63 degrees and the surface temperature values ranged between 80°C and 260°C. The optical camera resolution was 1024 × 512 with 14000 frames per second and 1 μs exposure time. The optical observation included the spreading length, splashing trends including the splashing angle, and transition regime behaviors. The main conclusions are as follows:

- Spreading lengths decreased by rising of the surface temperature until the end of the transition regime, which was defined as the sign of reaching the Leidenfrost point.
- The decrease of spreading diameter was 72.44% and 51.02% for the Weber numbers of 618 and 792, respectively.
- Liquid accumulation was observed at the surface temperature of 80°C due to low surface energy levels even though the surface temperature was higher than the boiling point of ethanol.
- For Experiment A, nucleation bubbles were seen at the surface temperature of 110°C while splashed droplets with non-uniform directions were observed for Experiment B. The main reason was the difference in the ethanol supply rate.
- Splashing angles were observed in the ranges of 170°C–185°C and 140°C–200°C for Experiments A and B, respectively. The decrease of splashing angle was a sign of transition regime.
- The post-transition regime was after the end of the transition regime and the Leidenfrost point was reached above 200°C for both experiments but it was started earlier in Experiment A due to the thermal balance between liquid ethanol supply rate and the surface energy level.
- Experiment A had a nearly 46.4% smaller spreading length than Experiment B. The minimum spreading lengths were nearly 0.2 and 0.4 mm whilst the maximum lengths were approximately 0.7 and 0.8 for Experiments A and B, respectively.

In addition to the mentioned conclusions, further studies can make significant contributions for a better understanding of droplet train impingement on the heated surface. For example, the impacts of various surface roughness values or specific surface modifications on boiling trends can be investigated. Also, different impingement angles (incline degrees) can be applied to see their impacts on the transition regime. Their time-dependent changes can be predicted via extrapolative prediction tools like in [16]. Moreover, at high frequency like in this study, smaller and greater Weber numbers can be examined because they also affect the boiling trends and behaviors, especially in transition and post-transition regimes. The statistical analysis can be done with image processing tools.

Acknowledgement: The authors would like to thank the funding supports from the School of Mechanical and Aerospace Engineering, Nanyang Technological University. B. B. Kanbur is the Mistletoe Research Fellow granted by the Momental Foundation.

Funding Statement: The authors received no specific funding for this study.

Conflicts of Interest: The authors declare that they have no conflicts of interest to report regarding the present study.

References

1. Yarin, A. L., Weiss, D. A. (1995). Impact of drops on solid surfaces: Self-similar capillary waves, and splashing as a new type of kinematic discontinuity. *Journal of Fluid Mechanics, 283,* 141–173. DOI 10.1017/S0022112095002266.

2. Tong, W., Qin, Z., Duan, F. (2018). Hydrodynamic pattern s of a droplet train impinging onto superheated nanotube surfaces. *17th IEEE Intersociety Conference on Thermal and Thermomechanical Phenomena in Electronic Systems (ITherm)*, pp. 838–841. California, USA.
3. Qiu, L., Dubey, S., Choo, F. H., Duan, F. (2017). The statistical analysis of droplet train splashing after impinging on a superheated surface. *Journal of Heat Transfer, 139,* 052201. DOI 10.1115/1.4035661.
4. Fathi, S., Dickens, P. M., Hague, R. J. M., Khodabkhski, K., Gilbert, M. (2008). Analysis of droplet train/moving substrate interactions in ink-jetting processes. *2008 International Solid Freeform Fabrication Symposium*, pp. 230–238. Texas, USA.
5. Sellers, S. M., Black, W. Z. (2008). Boiling heat transfer rates for small precisely placed water droplets on a heated horizontal plate. *Journal of Heat Transfer, 130,* 054504. DOI 10.1115/1.2884183.
6. Li, J., Zhang, H., Liu, Q. (2019). Dynamics of a successive train of monodispersed millimetric-sized droplets impact on solid surfaces at low weber number. *Experimental Thermal and Fluid Science, 102,* 81–93. DOI 10.1016/j.expthermflusci.2018.08.029.
7. Gradeck, M., Seiler, N., Ruyer, P., Maillet, D. (2013). Heat transfer for leidenfrost drops bouncing onto a hot surface. *Experimental Thermal and Fluid Science, 47,* 14–25. DOI 10.1016/j.expthermflusci.2012.10.023.
8. Dunand, P., Castanet, G., Gradeck, M., Lemoine, F., Maillet, D. (2013). Heat transfer of droplets impinging onto a wall above the leidenfrost temperature. *Comptes Rendus Mécanique, 341,* 75–87. DOI 10.1016/j.crme.2012.11.006.
9. Zhang, T., Muthusamy, J. P., Alvarado, J. L., Kanjikarat, A., Sadr, R. (2016). Numerical and experimental investigations of crown propagation dynamics induced by droplet train impingement. *International Journal of Heat and Fluid Flow, 57,* 24–33. DOI 10.1016/j.ijheatfluidflow.2015.10.003.
10. Shen, S., Tong, W., Duan, F. (2020). Hydrodynamic pattern transition of droplet train impinging onto heated titanium substrates with or without nanotube coating. *International Journal of Heat and Mass Transfer, 163,* 120409. DOI 10.1016/j.ijheatmasstransfer.2020.120409.
11. Kanbur, B. B., Hui, M. L. Z., Duan, F. (2020). Transient transition of high speed and high- frequency ethanol droplet train impingement on the heated indium tin oxide (ITO) surface. *5th International Conference on Smart and Sustainable Technologies (SpliTech)*, Split, Crotia.
12. Kanbur, B. B., Hui, M. L. Z., Duan, F. (2021). Transient hydrodynamic patterns of high weber number ethanol droplet train impingement on heated glass substrate. *International Communications in Heat and Mass Transfer, 126,* 105451. DOI 10.1016/j.icheatmasstransfer.2021.105451.
13. Qiu, L., Dubey, S., Choo, F. H., Duan, F. (2016). The transitions of time-independent spreading diameter and splashing angle when a droplet train impinging onto a hot surface. *RSC Advances, 6,* 13644–13652. DOI 10.1039/C5RA26314J.
14. Qiu, L., Dubey, S., Choo, F. H., Duan, F. (2015). Splashing of high speed droplet train impinging on a hot surface. *Applied Physics Letters, 107,* 164102. DOI 10.1063/1.4934531.
15. Khavari, M., Sun, C., Lohse, D., Tran, T. (2015). Fingering patterns during droplet impact on heated surfaces. *Soft Matter, 11,* 3298–3303. DOI 10.1039/C4SM02878C.
16. Tanis-Kanbur, M. B., Kumtepeli, V., Kanbur, B. B., Ren, J., Duan, F. (2021). Transient prediction of nanoparticle-laden droplet drying patterns through dynamic mode decomposition. *Langmuir, 37,* 2787–2799. DOI 10.1021/acs.langmuir.0c03546.